A NUMERICAL ESTIMATION OF DIFFUSION THERMO AND THERMAL DIFFUSION EFFECTS OF AN UNSTEADY MHD FLOW OF MAXWELL FLUID OVER A POROUS VERTICAL SHEET WITH THERMAL RADIATION AND CHEMICAL REACTION

Gangadhar Goddubarla 1* SharathBabu Kanday Rao[2] Srinivasa Kumar Vajha[3]

[1]Department of Mathematics, Malla Reddy Engineering College (Autonomous), Secunderabad, Pincode-500100, Telangana. India.
[2]Department of Mathematics, Matrusri Engineering College, Hyderabad, Pincode-500059Telangana. India.
[3]Department of Mathematics, JNTUH College of Engineering, Kukatpally, Pincode-500085, Hyderabad, Telangana. India.

Abstract: In this study, we have examined the effects of Diffusion thermal and thermal diffusion on MHD mixed convective flow of Maxwell fluid past a porous vertical stretching sheet in the presence of thermal radiation and chemical reaction is investigated. The governing equations of continuity, momentum, and energy are reduced to ordinary differential equation forms by introducing a similarity transformation. Numerical solutions of these equations are obtained by the RungeKutta fourth-order method along with the shooting technique, and the results obtained for different governing flow parameters are drawn graphically, and their effects on velocity, temperature, and concentration profiles are discussed. The values of the skin friction coefficient, Nusselt number coefficient, and Sherwood number coefficient are presented in the table. A comparison with previously reported data is made, and an excellent agreement is noted. The objectives of the present work are to investigate the effect of the Deborah numbers (De), Hartman electric number (Ha), Reynolds number (Rew), and Prandtl number (Pr) on the velocity and temperature fields. As an important outcome, it is observed that increasing the Hartman number reduces the velocity values while increasing the Deborah number has a negligible impact on the velocity increment.

Key words: mixed convective flow, Maxwell fluid, nonlinear thermal radiation, porous sheet.

1. Introduction:

The growing trend in technical and industrial applications grabs the attention of researchers to analyze mathematical models for non-Newtonian fluids. There are various applications of non-Newtonian liquids such as in metal extrusion, spinning of metals, lubricant manufacturing for

multiple vehicles, the distillation of molten metal from non-metallic insertion, manufacturing of shoes (to protect feet from injuries, the shoe needs to be packed with a specific non-Newtonian fluid), and food and medicine industries, and as a coolant. With the passage of time, various researchers have presented mathematical models of non-Newtonian fluids for analyzing the characteristics of these fluids.

Maxwell was the first to model a non-Newtonian fluid; its examples include polymer extrusion, nuclear reactor emergency cooling systems, food processing, and thermal welding. As the authors know, Maxwell fluid's steady-state boundary layer flow across a porous flat plate with the above-mentioned physical consequences has yet to be documented in the literature. Many authors have conducted a study using different geometries and parameters. But they have yet to study a porous flat plate combining thermal radiation, MHD, and heat generation over a Maxwell fluid flow with a moving velocity in the boundary condition. The Maxwell model is one such important subclass of mathematical models. Various researchers apply this model under different flow circumstances. Zierep and Fetecau [1] analyzed the energetic balance for Rayleigh–Stokes's first and second problems of the Maxwell fluid under the effect of various initial and boundary conditions. Fetecau et al. [2] also presented an unsteady flow for the Maxwell fluid of fractional derivatives under the influence of an accelerating plate with constant speed. In this examination, they solved the modeled equations by employing a combination of joint Fourier sine, and Laplace transforms and discussed various cases for the flow system. Renardy and Wang [3] addressed the boundary layer flow for the Maxwell fluid. In this study, these authors investigated that the boundary layer is basically of two types: the stress boundary layer and the Prandtl boundary layer. Hayat et al. [4] investigated the effect of mass transfer on the inaction point flow for Maxwell liquid. Hayat et al. [5] also explored the impact of the transmission of mass on a time-dependent MHD flow past a stretched surface in 2D for Maxwell flow. In this analysis, they have determined the series solution for a modeled problem by employing HAM. Abbasbandy [6] carried out analytical and numerical solutions for the MHD Maxwell fluid of Falkner–Skan flow. Mustafa et al. [7] discussed steady flow for visco-elastic Maxwell nanofluid. This study used an exponentially stretched surface subjected to heat convection. Awais et al. [8] addressed the boundary layer flow of Maxwell nanofluid with heat generation and heat absorption. In this investigation, the authors also conducted a comparative study regarding the numerical and analytical solutions of the modeled problem. Ramzan et al. [9] discussed Dufour and Soret effects for a mixed convection flow of

Maxwell nanofluid over a vertical porous surface extending outward and obtained an optimal solution to the modeled problem using the BVPh. 2.0 Mathematica Package.

The study of fluid flows and energy in a non-Newtonian fluid has gathered considerable notice due to its many engineering applications. The majority of investigations in the literature involve conventional Newtonian fluids. It is common knowledge that the bulk of fluids encountered in non-Newtonian is the process of terms under parameter estimations. Oil engineering, biology, physiology, technology, and industry utilize these fluids. Maxwell fluids are a subclass of non-Newtonian fluids that accurately capture fluids' pseudo-plastic and dilatant properties. Adegbie et al. [10] discovered the behaviour of heat and mass transport in Maxwell fluid flow with the impact of thermo-physical parameters over a flat melting surface. Mustafa et al. [11] researched the flux as non-Fourier in thermal variables for the rotation of Maxwell fluid flow. It was derived by Shafique et al. [12] within the context of a rotating frame. Olabode et al. [13] studied Maxwell fluids with the impact on temperature-dependent variable characteristics and the influence of quadratic thermo-solutal convection. Heyhat and Khabazi [14] observed the non-isothermal flow of Maxwell fluid over fixed horizontal plates influenced by a transverse magnetic field. In the above articles, authors used Maxwell fluid on different geometries but not on a flat plate. So, Maxwell fluid flow on the flat plate must be included with the existing.

Porous medium is a material that contains either connected or unconnected voids (pores) spread in a regular or random pattern. These pores may contain various fluids, including air, water, oil, etc. If pores represent a percentage of the bulk volume, a composite network capable of fluid transport can be constructed. The permeability of the porous medium was the partial and overall bulk quantity of volume. The structure of the porous material determines permeability, a measure of the material's mean square pore diameter. The following authors included porous media in their study. Bhattacharyya [15] investigated chemically reactive flow's firstorder diffusion equations across a porous flat plate focused on force and changing wall concentration. Sadia et al. [16] examined the convection of energy–mass transfer with generalized Maxwell fluid impact, chemical reaction and exponential heating utilizing fractional derivatives models such as Caputo–Fabrizio. Shenoy [17] researched heat transport in non-Newtonian fluids throughout porous media. In the above research, a few authors have used a porous medium in different geometries, especially not in flat plates over Maxwell fluid.

The study of heat transfer with chemical reactions in the presence of nanofluids is of great practical importance to engineers and scientists because of its almost universal occurrence in many branches of science and engineering. Possible applications of this type of flow can be found in many industries. In many engineering applications such as nuclear reactor safety, combustion systems, solar collectors, metallurgy, and chemical engineering, many transport processes are governed by the joint action of the buoyancy forces from both thermal and mass diffusion in the presence of chemical reaction effects. Radiative flows are encountered in countless industrial and environmental processes such as heating and cooling chambers, fossil fuel combustion and energy processes, evaporation from sizeable open water reservoirs, astrophysical flows, and solar power technology. However, the thermal radiation heat transfer effects on different flows are significant in high-temperature processes and space technology. Maatoug et al. [18] have studied Variable chemical species and thermo-diffusion Darcy– Forchheimer squeezed flow of Jeffrey nanofluid in a horizontal channel with viscous dissipation effects. Omar et al. [19] have analyzed Hall Current and Soret Effects on Unsteady MHD Rotating Flow of Second-Grade Fluid through Porous Media under the Influences of Thermal Radiation and Chemical Reactions. Deepthi et al. [20] have discussed the Recent Development of Heat and Mass Transport in the Presence of Hall, Ion Slip, and Thermo Diffusion in Radiative Second Grade Material: Application of Micromachines. Aruna et al. [21] have possessed an unsteady MHD flow of a second-grade fluid passing through a porous medium in the presence of radiation absorption exhibits Hall and ion slip effects. The chemically reactive second grade via porous saturated space was investigated by Raghunath et al. [22] using a perturbation technique. Raghunath et al. [23] have investigated the effects of Soret, Rotation, Hall, and Ion Slip on the unsteady flow of a Jeffrey fluid through a porous medium. Raghunath and Mohanaramana [24] have researched Hall, Soret, and rotational effects on unsteady MHD rotating flow of a second-grade fluid through a porous media in the presence of chemical reaction and aligned magnetic field.

The principal aim of the present work is to study the impacts of thermal diffusion and diffusion thermo on MHD mixed convective flow of Maxwell fluid past a porous vertically stretching sheet in the presence of thermal radiation and chemical reaction. The governing equations can obtain similarity transformations that reduce a system of governing partial differential equations and associated boundary conditions to a system of ordinary differential equations. This transformation derives third-order and second-order ordinary differential equations corresponding to momentum,

energy, and concentration equations. These equations are solved with the help of Runge Kutta's fourth order and shooting technique. The effects of different flow parameters on velocity, temperature, and concentration profiles are investigated and analysed with the help of a graphical representation.

2. Problem Formulation

We consider 2D viscous incompressible laminar flow with heat transmission of a non-Newtonian electrically conducting Maxwell Nanofluid through a porous medium and also the combined effects of mixed convection with convective boundary conditions. Flow is considered on a stretching sheet in the presence of Dufour and Soret effects and variable thermal conductivity. A uniform magnetic field $B = \frac{B_0}{\sqrt{1-\chi t}}$ is applied in opposite to the direction of the fluid flow. The stretched sheet of velocity is $U_w = \frac{cx}{\sqrt{1-\chi t}}$ and $\nu = \nu_w = \frac{\nu_0}{\sqrt{1-\chi t}}$ where c, χ are positive constants. In addition, all physical attributes related to the formula are measured to be constant. The geometry of this modelling can be displayed in Figure 1. Bossineq approximation is taken for both energy or temperature and concentration profiles. The continuity, momentum, energy and concentration equations governing such type of flow in the presence of chemical reaction are written as below:

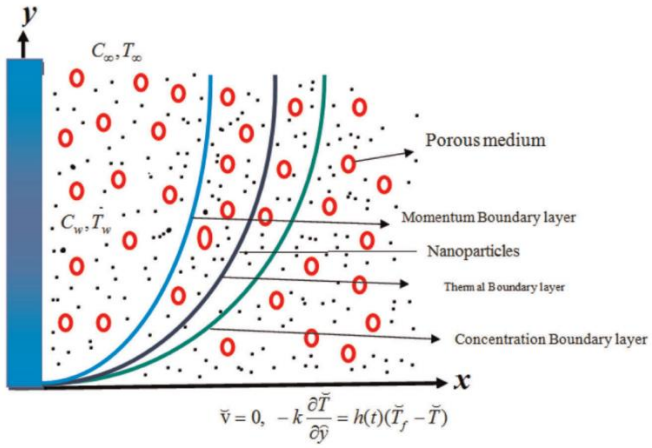

Figure: 1. Physical configuration of the Problem

$$\frac{\partial u}{\partial x}+\frac{\partial u}{\partial y}=0 \tag{1}$$

$$\frac{\partial u}{\partial t}+u\frac{\partial u}{\partial x}+v\frac{\partial u}{\partial y}=\nu\frac{\partial^2 u}{\partial y^2}-\lambda_1\left(u^2\frac{\partial^2 u}{\partial x^2}+v^2\frac{\partial^2 u}{\partial y^2}+2uv\frac{\partial^2 u}{\partial x\,\partial y}\right)+ g\beta_T\left(T-T_\infty\right)+\ g\beta_C\left(C-C_\infty\right)-\sigma\frac{B_0(t)}{\alpha}-\ \frac{\vartheta}{k}u \tag{2}$$

$$\frac{\partial T}{\partial t}+u\frac{\partial T}{\partial x}+v\frac{\partial T}{\partial y}=\alpha_m\left(\frac{\partial^2 T}{\partial y^2}\right)+\tau\left(D_B\frac{\partial C}{\partial y}\frac{\partial T}{\partial y}+\frac{D_T}{T_\infty}\left(\frac{\partial T}{\partial y}\right)^2\right)-\frac{1}{(\rho Cp)}\frac{\partial q_r}{\partial y}+ \frac{\mu}{(\rho c)_f}\left(\frac{\partial u}{\partial y}\right)^2+\frac{D_m k_T}{c_s c_p}\frac{\partial^2 C}{\partial y^2} \tag{3}$$

$$\frac{\partial C}{\partial t}+u\frac{\partial C}{\partial x}+v\frac{\partial C}{\partial y}=\frac{D_m k_T}{T_m}\frac{\partial T^2}{\partial y^2}+D_B\left(\frac{\partial^2 C}{\partial y^2}\right)+\frac{D_T}{T_\infty}\left(\frac{\partial T^2}{\partial y^2}\right)-K_0\left(C_w-C_\infty\right) \tag{4}$$

For this flow, corresponding boundary conditions are

$$\begin{aligned} &u=U_w(x,t),\quad v=0,\ -k\frac{\partial T}{\partial y}=h(t)\left(T_f-T_\infty\right),\quad C=C_w \qquad \text{at } y=0\\ &u\to 0,\quad v\to 0,\quad T\to T_\infty \qquad C\to C_\infty \qquad\qquad \text{as } y\to\infty \end{aligned} \tag{5}$$

where (u,v) are the components of velocity in x and y directions, λ_1 is the relaxation time, υ is the kinematic viscosity, κ_0 is the chemical reaction parameter, g is the gravitational acceleration, β_T is the thermal expansion coefficient, (T,C) are fluid temperature and concentration, and DB and DT are Brownian and thermophoretic coefficient, the density of the fluid.

The radiative heat flux q_r (using Roseland approximation followed [24]) is defined as

$$q_r=-\frac{4\sigma^*}{3k^*}\frac{\partial T^4}{\partial y} \tag{6}$$

where k^* is the mean absorption coefficient, and σ^* is the Stefan-Boltzmann constant.

We assume that the temperature variances inside the flow are such that the term T^4 can be represented as linear function of temperature. This is accomplished by expanding T^4 in a Taylor series about a free stream temperature T_∞ as follows:

$$T^4 = T_\infty^4 + 4T_\infty^3\left(T - T_\infty\right) + 6T_\infty^2\left(T - T_\infty\right)^2 + \ldots\ldots\ldots \tag{7}$$

After neglecting higher-order terms in the above equation beyond the first degree term in $\left(T - T_\infty\right)$, we get

$$T^4 \cong 4T_\infty^3 T - 3T_\infty^4 \tag{8}$$

Using (8) in (6) and then the substitution of its value in Eq. (3), gives

$$\frac{\partial q_r}{\partial y} = -\frac{16\sigma^* T_\infty^3}{3k^*}\frac{\partial^2 T}{\partial y^2} \tag{9}$$

Using (9), Eq. (3) can be written as

$$\frac{\partial T}{\partial t} + u\frac{\partial T}{\partial x} + v\frac{\partial T}{\partial y} = \alpha_m\left(\frac{\partial^2 T}{\partial y^2}\right) + \tau\left(D_B\frac{\partial C}{\partial y}\frac{\partial T}{\partial y} + \frac{D_T}{T_\infty}\left(\frac{\partial T}{\partial y}\right)^2\right) - \frac{1}{(\rho c)_f}\frac{16T_\infty^3\sigma^*}{\partial K^*}\left(\frac{\partial^2 T}{\partial y^2}\right) + \frac{\mu}{(\rho c)_f}\left(\frac{\partial u}{\partial y}\right)^2 + \frac{D_m k_T}{c_s c_p}\frac{\partial^2 C}{\partial y^2} \tag{10}$$

The following similarity variables are introduced for solving governing equations (2), (6) and (4) as

$$u = \frac{ax}{1-\chi t}f'(\eta),\ v = -\sqrt{\frac{a}{(1-\chi t)}}f(\eta),\ \eta = \sqrt{\frac{va}{1-\chi t}}y,\ \phi(\eta) = \frac{C - C_\infty}{C_w - C_\infty},$$

$$\theta(\eta) = \frac{T - T_\infty}{T_w - T_\infty},\ h(t) = \frac{d}{\sqrt{1-\chi t}}. \tag{11}$$

Substituting Eq. (11) into Eqs. (2), (3) and (4), we get the following system of non-linear ordinary differential equations

$$f''' - f'^2 + ff'' + \Lambda\left(2ff'f'' - f^2 f'''\right) - \delta\left(f' + \frac{1}{2}\eta f''\right) - (M+\beta)f' + \lambda(\theta + N\phi) = 0 \tag{12}$$

$$\left(1+\frac{4}{3}R_d\right)\theta'' - \delta \Pr\frac{1}{2}\eta\theta' - \Pr f\theta' + \Pr N_b\left(\theta'\phi' + \frac{N_t}{N_b}\theta'^2\right) - Ef'' + \Pr D_u\phi' = 0 \tag{13}$$

$$\phi'' - \delta \Pr\frac{1}{2}\eta\phi' - Sc\left(f\phi' + K\phi - Sr\phi'\right) + \frac{N_b}{N_t}\theta'' = 0 \tag{14}$$

The corresponding boundary conditions (5) become

$$\begin{aligned} &f(\eta) = S, \quad f'(\eta) = 1, \quad \theta'(\eta) = -\gamma(1-\theta(\eta)), \quad \phi(\eta) = 1 \qquad at \quad \eta = 0 \\ &f'(\eta) \to 0, \quad \theta(\eta) \to 0, \quad \phi(\eta) \to 0 \qquad as \quad \eta \to \infty \end{aligned} \tag{15}$$

where prime denotes differentiation with respect to η, and the significant thermophysical parameters indicating the flow dynamics are defined by

$\delta = \frac{c}{\chi}$ is the Unsteady Parameter,

$\Lambda = c\lambda_1$ is the Maxwell fluid parameter,

$\lambda = \left(\frac{g\beta_T(T_w - T_\infty)x}{U_w^2}\right)$ is the mixed convection parameter

$N = \frac{\beta_c(C_w - C_\infty)}{\beta_T(T_w - T_\infty)}$ is the Deborah Number

$\beta = c\lambda_1$ is the dimensionless bouncy parameter

$M = \frac{\sigma B_0^2}{\rho Cp}$ is the magnetic number

$N_b = \frac{\tau D_B(C_w - C_\infty)}{\nu}$ is the Brownian motion parameter

$N_t = \dfrac{\tau D_T (T_w - T_\infty)}{\alpha}$ is the thermophoresis parameter

$R_d = \dfrac{4\sigma^* T_\infty^3}{kk^*}$ is the radiation parameter

$\Pr = \dfrac{\nu}{\alpha} = \dfrac{\nu \rho C_p}{k}$ is the Prandtl number

$Sc = \dfrac{\nu}{D_B}$ is the Schmidt number

$\gamma = \left(\dfrac{h_f}{k} \sqrt{\dfrac{\nu}{\alpha}} \right)$ is the Biot number

$E_c = \dfrac{U_w^2}{C_p (T_w - T_\infty)}$ is the Eckert number

$K = \dfrac{R_C}{c}$ is the chemical reaction parameter

$Du = \dfrac{D_M k_T (C_w - C_\infty)}{C_S C_p \nu a^2 (T_w - T_\infty)}$ is the Diffusion thermo parameter

$S_r = \dfrac{D_m k_T (T_w - T_\infty)}{T_m \alpha_m (C_w - C_\infty)}$ is the Thermal diffusion parameter

The local skin friction coefficient Cf, the local Nusselt number Nu_x, and the local Sherwood number Sh_x are the physical quantities of relevance that influence the flow. These numbers have the following definitions:

$$C f = \frac{\tau_w}{\rho U_w^2}, \quad Nu_x = \frac{x q_w}{k (T_w - T_\infty)}, \quad Sh_x = \frac{x q_m}{D_B (C_w - C_\infty)} \tag{16}$$

The shear stress, heat, and mass flux are written as

$$\tau_w = \mu \left[\frac{\partial u}{\partial y} \right]_{y=0}, \quad q_w = -k \left[\frac{\partial T}{\partial y} \right]_{y=0}, \quad q_m = D_B \left[\frac{\partial C}{\partial y} \right]_{y=0} \tag{17}$$

The coefficient of skin friction, the Nusselt number, and the Sherwood number are all expressed in their non-dimensional versions in terms of the similarity variable as follows:

$$\mathrm{Re}_x^{1/2} Cf = f''(0), \quad \mathrm{Re}_x^{-1/2} Nu_x = -\left(1+\frac{4}{3}R_d\right)\theta'(0), \quad \mathrm{Re}_x^{-1/2} Sh_x = -\phi'(0) \tag{18}$$

3. Solution Methodology

As Equations. (12)–(14) with boundary conditions (15) are strongly non-linear, it is difficult or maybe impossible to find the closed form solutions. Accordingly, these boundary value problems are solved numerically by using the conventional fourth-order RK integration scheme along with the shooting technique.

The first task to carry out the computation is to convert the boundary value problem to an initial value problem.

Let by using the following notations:

$$f = y_1,\ f' = y_2, f'' = y_3,\ f''' = y_3',\ \ \theta = y_4,\ \theta' = y_5, \theta'' = y_5',\ \ \phi = y_6,\ \phi' = y_7, \phi'' = y_7'. \tag{19}$$

By using the above variables, the system of first-order ODEs is

$$y_1' = y_2, \tag{20}$$

$$y_2' = y_3, \tag{21}$$

$$y_3' = \frac{1}{\left(1+\Lambda y_1^2\right)}\left(y_2^2 - y_1 y_3 - 2\Lambda y_2 y_3 + \delta\left(y_2 + \frac{1}{2}\eta y_3\right) + \left(M+\beta\right)y_2 - \lambda\left(y_4 + N y_6\right)\right), \tag{22}$$

$$y_4' = y_5, \tag{23}$$

$$y_5' = \frac{1}{1+R_d}\left(\frac{1}{2}\delta\eta \,\mathrm{Pr}\, y_5 + \mathrm{Pr}\, y_1 y_5 - \mathrm{Pr}\, N_b\left(y_5 y_7 + \frac{Nt}{Nb}\left(y_5\right)^2\right) + Ec y_3 - \mathrm{Pr}\ Du\ y_7\right) \tag{24}$$

$$y_6' = y_7, \tag{25}$$

$$y_7' = \frac{1}{2}\delta\eta \,\mathrm{Pr}\, y_7 + Sc\left(y_1 y_7 + R_c y_6 - S r y_7\right) - \frac{N_b}{N_t} y_5' \tag{26}$$

The boundary conditions are given as

$$\begin{aligned} &y_1(0) - S = 0, \quad y_2(0) - 1 = 0, \quad y_5(0) + \gamma\left(1 - y_4(0)\right) = 0, \quad y_6(0) - 1 = 0 \\ &y_2(\infty) = 0, \quad y_4(\infty) = 0, \quad y_6(\infty) = 0 \end{aligned} \tag{27}$$

The boundary conditions in Equation (27) are utilized via use a finite value of η_{max} as given

$$f'(\eta_{\max}) \to 0,\ \theta'(\eta_{\max}) \to 0,\ \phi'(\eta_{\max}) \to 0. \tag{28}$$

The step is taken $\Delta\eta = 0.001$ and convergent criteria is 10^{-6} for the desired accuracy

4. Code validation

We checked the accuracy of current outcomes with previous literature in the limited case and obtained a fantastic agreement. Table 1 displays a comparison of numeric outcome for f″(0) numerous values of the magnetic field parameter with the published result of Venkata Ramudu et al. [15] with an outstanding agreement.

5. Result and Discussion

In the current work, the MHD flow of Maxwell nanoparticles with convective boundary conditions is examined. Also, heat transfer and viscous dissipation are considered. To show the effect of some pertinent physical aspects, the obtained result is computed. The outcome of these physical parameters is elaborated through graph 2–26 and in Table 2, we computed the value of $\mathrm{Re}_x^{1/2} Cf_x$, $\mathrm{Re}_x^{-1/2} Nu_x and$ $\mathrm{Re}_x^{-1/2} Sh_x$ for entrenched flow variables.

For different values of the magnetic parameter M, the velocity and the temperature profiles are plotted in Figure 2 and 3 respectively. From Figure 2, it is clear that an increase in the magnetic parameter M leads to a fall in the velocity. The effects of the magnetic parameter to increase the temperature profiles are noticed from Figure 3. The presence of Lorentz force retards the force on the velocity field and therefore the velocity profiles decreases with the effect of magnetic parameter. This force has the tendency to slow down the fluid motion and the resistance offered to the flow. Therefore, it is possible for the increase in the temperature.

Figures 4–5 are displayed to study the velocity f′(η), and temperature θ(η) profiles for the numeric value of porosity parameter β. It is observed that the velocity field is a declining function of porosity variable β. actually, a higher value of β causes a stronger restriction and growing thickness of porous medium due to which the fluid flow motion depreciates. So, the velocity of the fluid reduces with an increased value of β. But, the opposite behavior is noted in θ (η).

The velocity $f'(\eta)$, temperature $\theta(\eta)$, and concentration $\phi(\eta)$, profiles for the diverse values of an unsteadiness parameter δ are evaluated in Figures 6–8. It is seen that from Figures 6 and 8, an increment in the value of δ obtains diminution in the velocity field and concentration distribution as the momentum and solute boundary layer. There is an increment in the temperature of nanoparticles via a larger value of δ as the thermal boundary layer.

The impact of fluid parameter λ for velocity $f'(\eta)$, temperature field $\theta(\eta)$ and concentration of nanoparticles $\phi(\eta)$ is considered in Figures 9–11. It is clearly noticed from these figures the waning function of the fluid parameter. It can be observed that the influence of enhancing the estimations of fluid parameters ε is to depreciate the $f'(\eta)$, field and is associated with boundary layer thickness depreciating. The $\theta(\eta)$ and $\phi(\eta)$ both are showing as opposite behavior with increasing value of the fluid parameter.

Temperature is enhanced when the Brownian motion parameter Nb is increased. Larger the Brownian motion parameter, lower the viscous force and higher the Brownian diffusion coefficient which results an enhancement in the thermal boundary layer thickness and temperature and this phenomenon can be observed in Figure 12. From Figure 13, it is observed that the nanoparticle concentration decreases with an increment in Nb.

Figures 14 and 15 illustrate the effect of thermophoresis parameter Nt on the temperature and the nanoparticles concentration profile. One can observe that temperature fields' increase with an enhancement in Nt. Thermophoresis parameter plays an important role in the heat transfer flow. Thermophoresis force enhances when Nt is increased which tends to move the nanoparticles from the hot region to the cold and as a result the temperature and the boundary layer thickness increase. The opposite behavior has observed in figure 15, in the case of concentration field.

Figure 16-17 illustrates the influence of the radiation parameter (Rd) on the temperature and concentration profiles. It is apparent that an increase in the radiation parameter results in a corresponding temperature rise. The observed phenomenon can be attributed to the liberation of heat energy into the fluid, consequent to increased thermal radiation. The phenomenon of reversal behavior has been observed in the field of concentration. The temperature field's effects, as influenced by the Eckert number Ec are presented in Figure 18. The augmentation of the Eckert number results in an elevation of the temperature field.

Figure 19-20 depicts the effect of Dufour parameter on temperature and concentration profiles respectively. As the Dufour parameter increases, the energy or temperature and concentration profiles are increases. The Dufour number denotes the contribution of the concentration gradients to the thermal energy flux in the flow. It can be seen that an increase in the Dufour number causes a rise in temperature.

Figure 21, and 22 illustrate that the Soret number Sr decreases temperature profile while there is an increase in concentration profile and boundary layer thickness. Higher temperature difference and a lower concentration difference are observed because of increasing values of the Soret number. This variation in the temperature and concentration differences is liable for the decrease in the temperature and an increase in the concentration. It is also noticed that the Dufour and Soret numbers have fairly contrary effects for temperature and nanoparticle concentration fields.

The underlying cause is the transformation of mechanical energy into thermal energy. The observed phenomenon is solely attributed to the dissipation of thermal energy. Figure 23 illustrates the influence of chemical response K on the concentration profile. The diminishment of the concentration boundary layer is directly related to the increase in the chemical reaction parameter R*c*. The impact of Schmidt number on the concentration profile is illustrated in Figure 24. There exists a correlation between the diffusivity of momentum and the diffusivity of mass. A decrease in the Schmidt number results in a decay of the concentration profile.

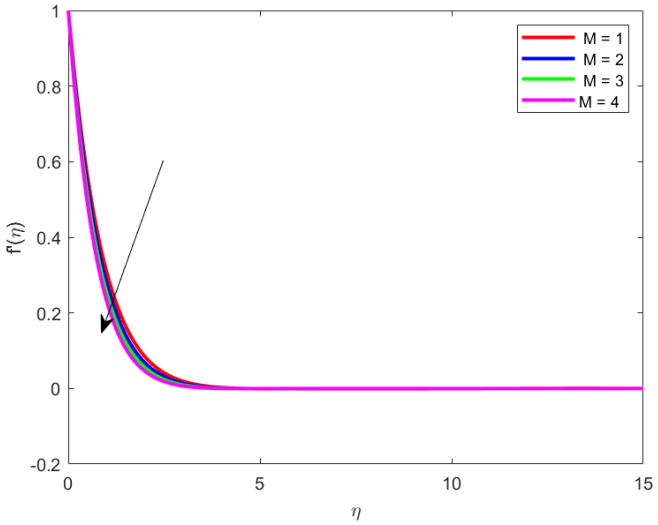

Figure2. Effect of magnetic parameter M on velocity profiles

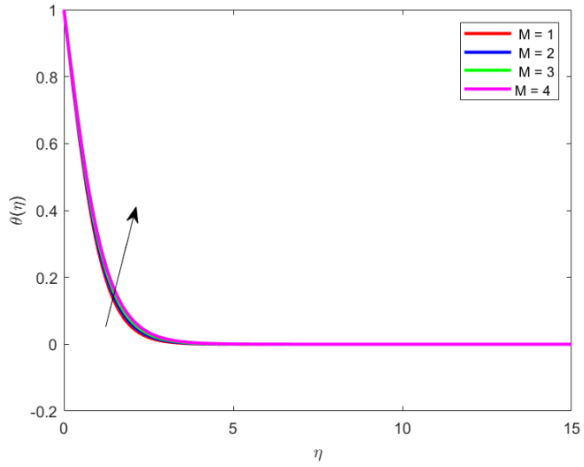

Figure3. Effect of M on Temperature profiles

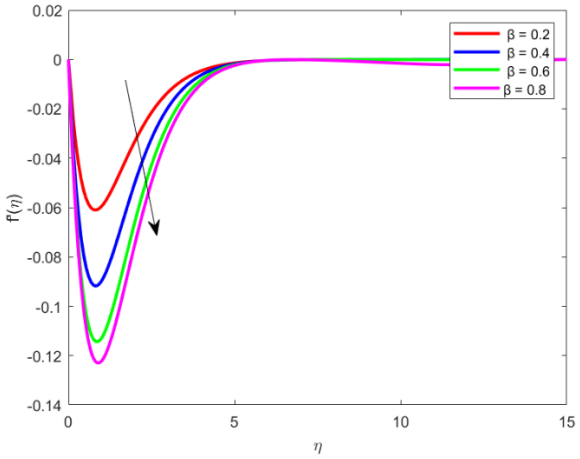

Figure4. Effect of porous parameter β on velocity profiles

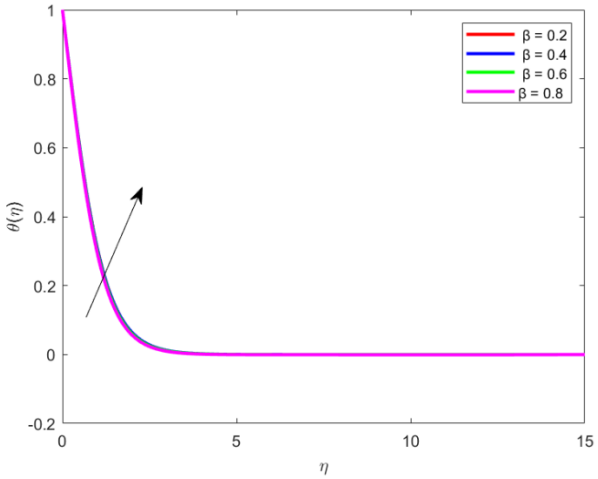

Figure5. Effect of β on Temperature profiles

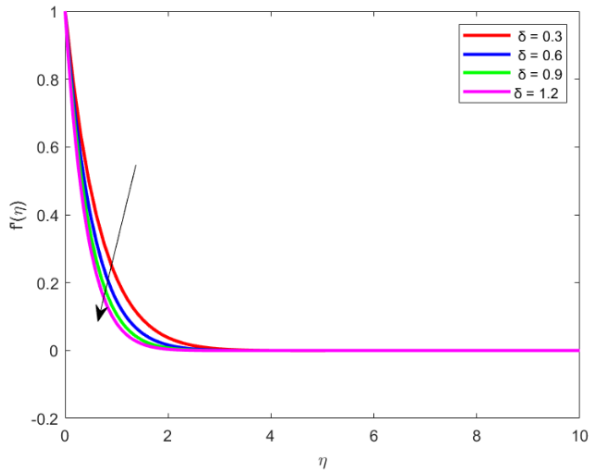

Figure6. Effect of unsteady parameter δ on velocity profiles

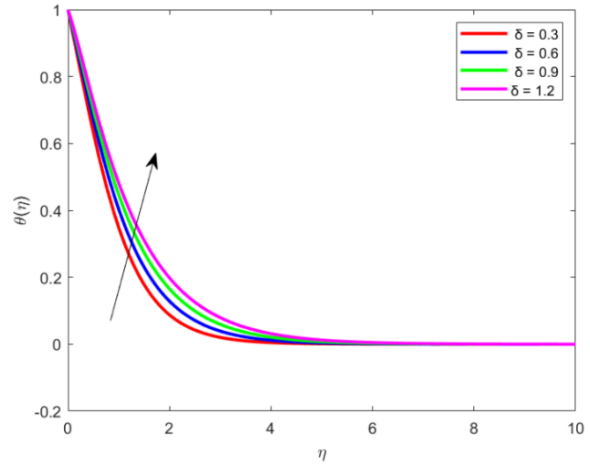

Figure7. Effect of unsteady parameter δ on Temperature profiles

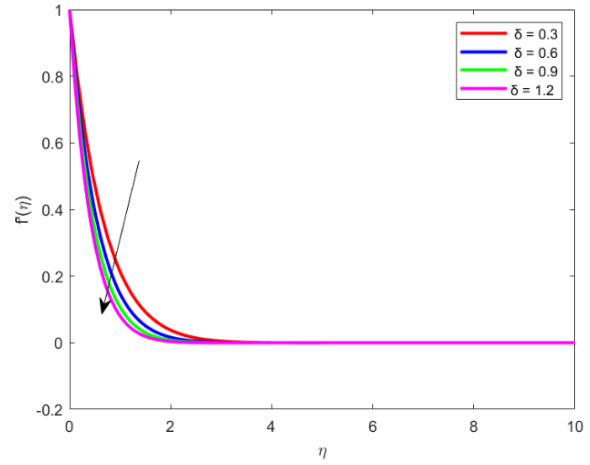

Figure8. Effect of unsteady parameter δ on Concentration profiles

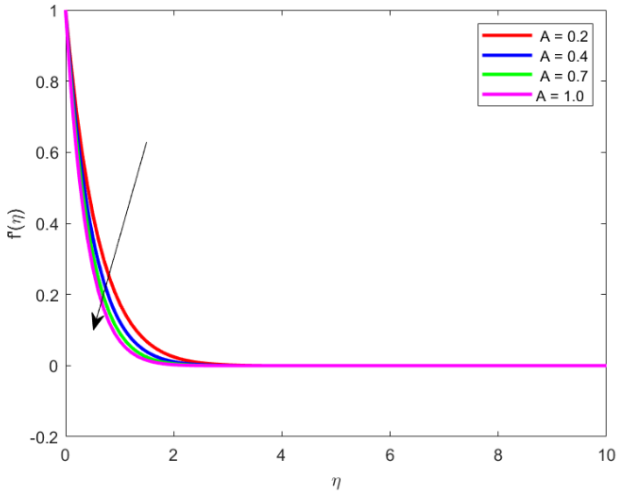

Figure9. Effect of Maxwell fluid parameter ʌ on velocity profiles

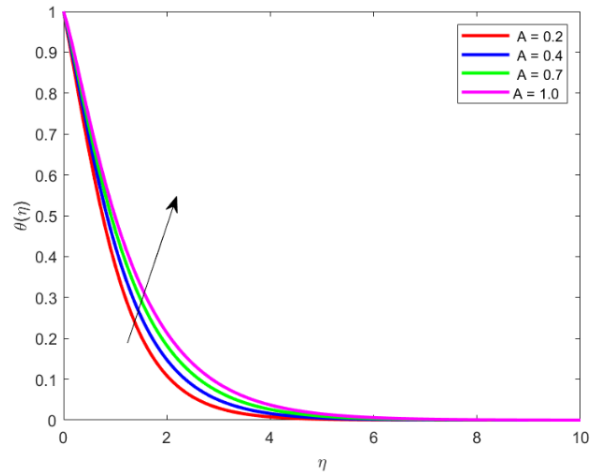

Figure10. Effect of Maxwell fluid parameter ʌ on Temperature profiles

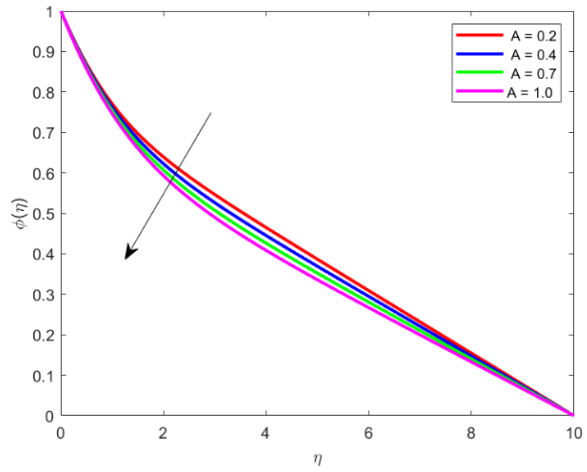

Figure11. Effect of Maxwell fluid parameter ʌ on Concentration profiles

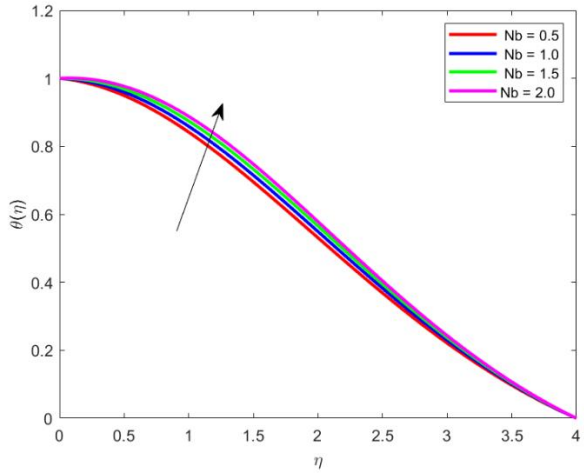

Figure12. Effect of Brownian motion parameter Nb on Temperature profiles

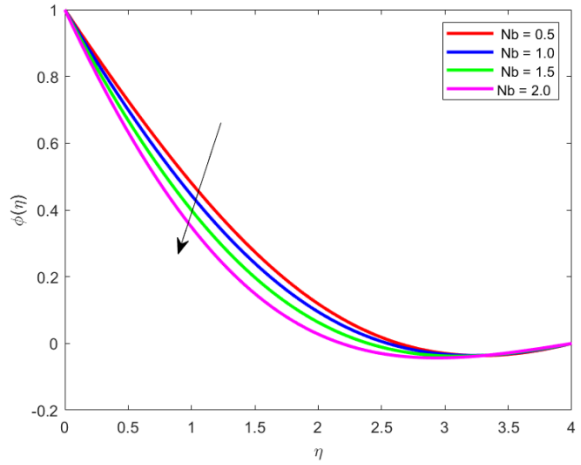

Figure13. Effect of Brownian motion parameter Nb on Concentration profiles

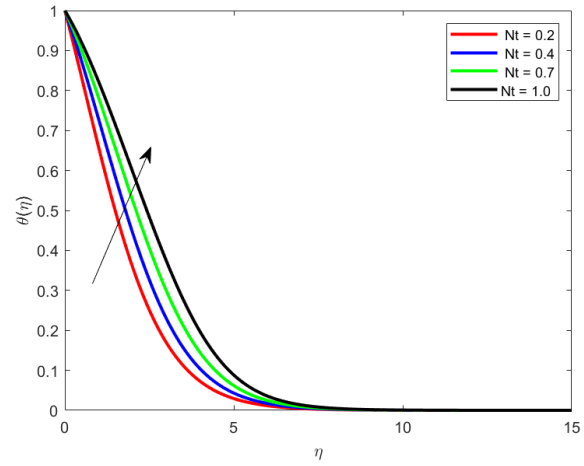

Figure14. Effect of Brownian motion parameter Nt on Temperature profiles

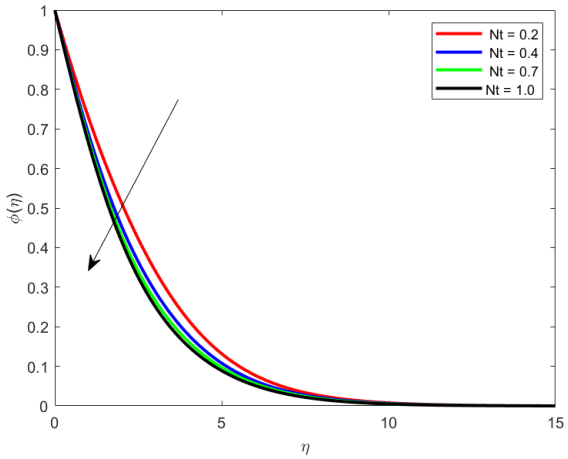

Figure15. Effect of Brownian motion parameter Nt on Concentration profiles

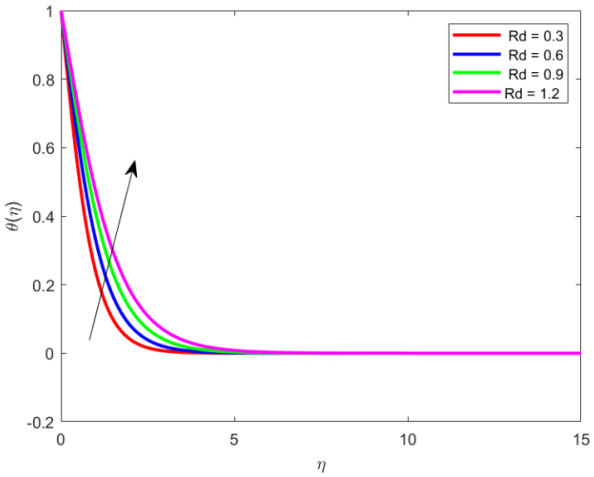

Figure16. Effect of Radiation parameter Rd on Temperature profiles

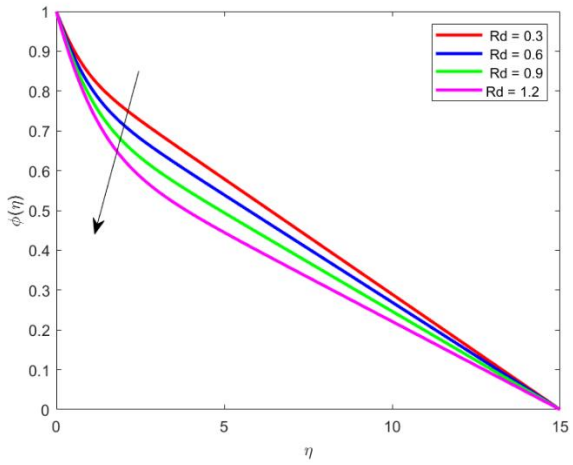

Figure17. Effect of Radiation parameter Rd on Concentration profiles

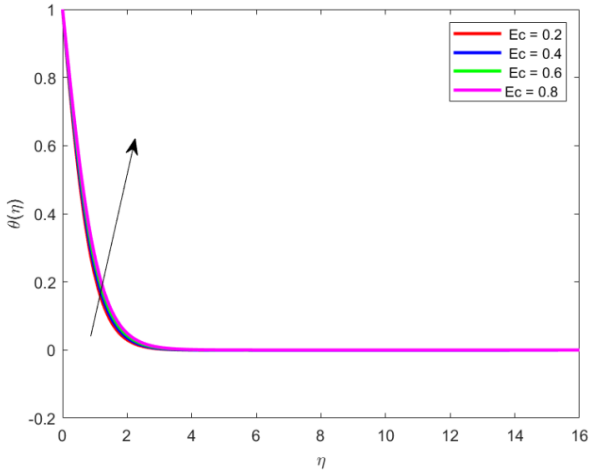

Figure18. Effect of Ekert number Rd on Temperature profiles

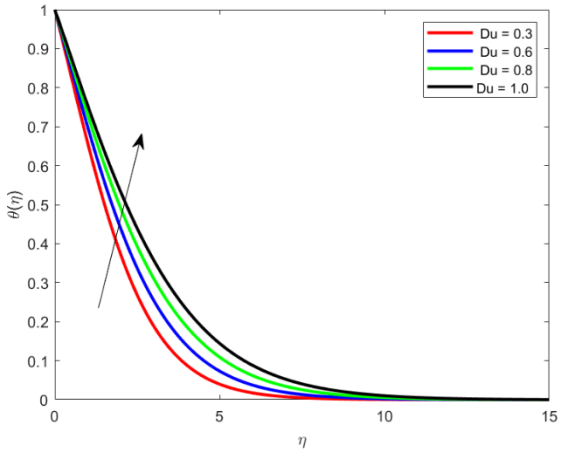

Figure19. Effect of Diffusion thermo Parameter Du on Temperature profiles

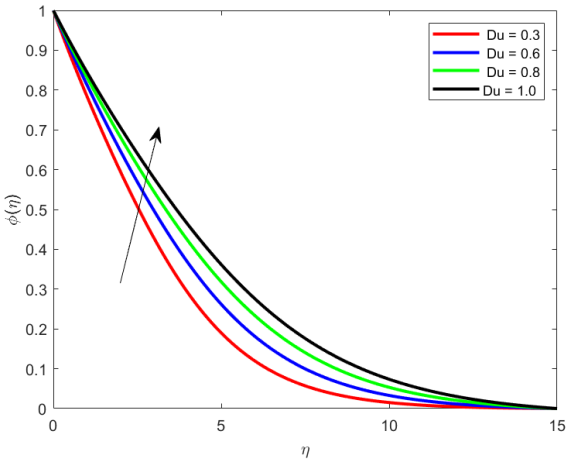

Figure20. Effect of Diffusion thermo Parameter Du on Concentration profiles

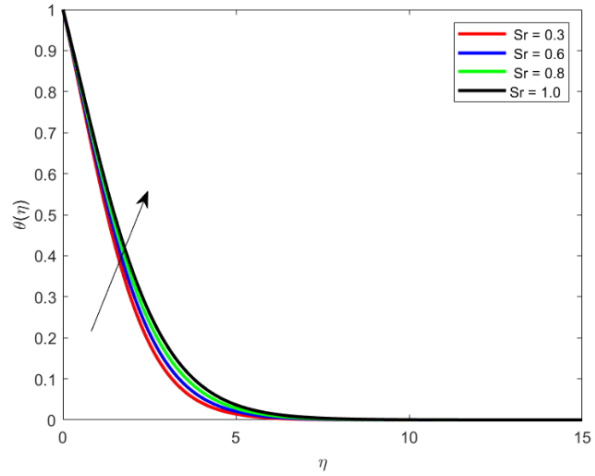

Figure21. Effect of Thermal Diffusion Parameter Sr on Temperature profiles

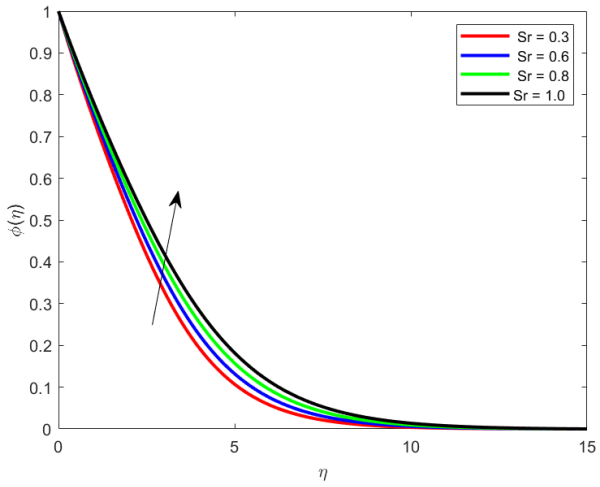

Figure22. Effect of Thermal Diffusion Parameter Sr on Concentration profiles

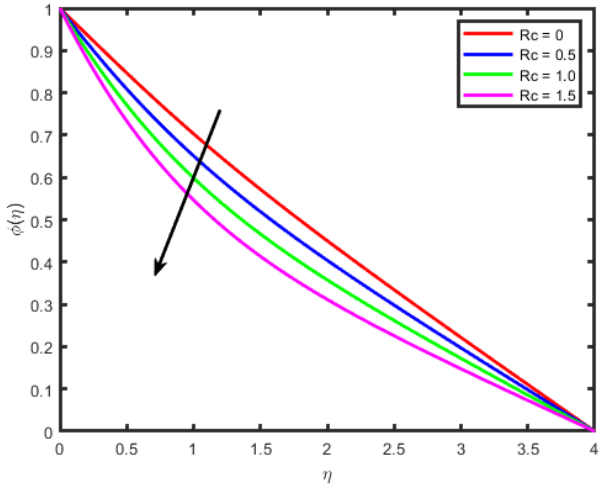

Figure23. Effect of chemical reaction K on Concentration profiles

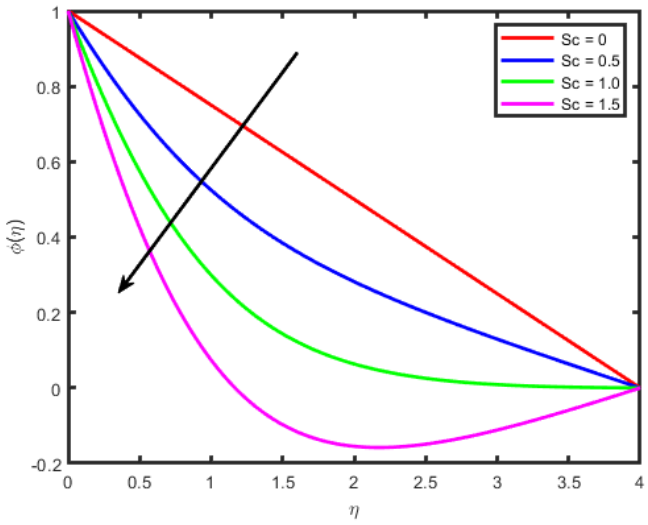

Figure24. Effect of Schmidt number Sc on Concentration profiles

Table: 1. Comparison of Skin friction coefficient $f''(0)$for different values of M when ʌ=β=0

M	Venkata Ramudu et al. [15]	Present Study
0.5	-0.376895	-0.37698
1.0	-0.529305	-0.529386
1.5	-0.654598	-0.654587

TABLE 2: Computation of $\mathrm{Re}_x^{1/2} Cf_x$, $\mathrm{Re}_x^{-1/2} Nu_x$ *and* $\mathrm{Re}_x^{-1/2} Sh_x$ for different parameters

Nb	Nt	Sc	Rc	Du	Sr	M	ʌ	$\mathrm{Re}_x^{1/2} Cf_x$	$\mathrm{Re}_x^{-1/2} Nu_x$	$\mathrm{Re}_x^{-1/2} Sh_x$
						1		1.1134	0.8973	0.2534
						2		1.4476	0.7636	0.6547
						3		1.8764	0.5436	0.9836
0.5								1.6534	0.8272	0.7383
1.0								1.1836	0.7262	0.9878
1.5								0.9909	0.5632	1.3536
	0.2							1.2341	0.9847	0.3647
	0.4							1.4285	0.7636	0.1094
	0.7							1.6298	0.5398	0.0946
		0.5						1.1087	0.1131	0.1241
		1.0						1.3592	0.1090	0.1187
		1.5						1.7152	0.0893	0.2127
			0.5					1.2504	0.1125	0.2170
			1.0					1.4921	0.1083	0.2179
			1.5					1.8230	0.0772	0.3084

				0.3				1.0085	0.7104	0.3759
				0.6				1.0478	0.6827	0.2983
				0.8				1.0985	0.6556	0.2764
					0.3			0.9458	0.8726	0.2756
					0.6			0.7249	0.8198	0.4672
					0.8			0.4763	0.7864	0.6728
							0.2	1.5138	0.1096	0.3787
							0.4	1.5999	0.0990	0.1097
							0.7	1.9182	0.0463	0.2144

6. Conclusion

In this work, investigated the effects of Thermal diffusion and Diffusion thermo on MHD mixed convective flow of Maxwell fluid past a porous vertical stretched surface in presence of thermal radiation and chemical reaction. The resulting partial differential equations, which describe the problem, are transformed in to ordinary differential equations by using introducing a similarity transformation and then solved by numerically by fourth order Runge-Kutta method along with shooting technique. Velocity, temperature and concentration profiles are presented graphically and analyzed. The findings of the numerical results can be summarized as follows:

- **i.** A stronger magnetic parameter M results in an increase in the temperature, concentration and transvers velocity
- **ii.** Thermal and concentration boundary layer thickness increase with the increase in thermophoresis parameter.
- **iii.** Brownian motion parameter has opposite effect on temperature and concentration fields.
- **iv.** The temperature distribution is a reducing function of thermal radiation Rd and Eckert number E
- **v.** The fluid temperature and concentration are enhances with increasing the Soret and Dufour specifications.

References

[1].J. Zierep and C. Fetecau, “Energetic balance for the Rayleigh–Stokes problem of a Maxwell fluid,” Int. J. Eng. Sci. 45, 617–627 (2007).

[2]. C. Fetecau, M. Athar, and C. Fetecau, "Unsteady flow of Maxwell fluid with fractional derivative due to a constantly accelerating plate," Comput. Math. Appl. 57, 596–603 (2009).
[3]. M. Renardy and X. Wang, "Boundary layers for the upper convected Maxwell fluid," J. Non-Newtonian Fluid Mech. 189-190, 14–18 (2012).
[4]. T. Hayat, M. Awais, M. Qasim, and A. A. Hendi, "Effects of mass transfer on the stagnation point flow of an upper convected Maxwell fluid," Int. J. Heat Mass Transfer 54(15-16), 3777–3782 (2011).
[5]. T. Hayat, M. Awais, and M. Sajid, "Mass transfer effects on the unsteady flow of UCM fluid over a stretching sheet," Int. J. Mod. Phys. B 25, 2863–2878 (2011).
[6]. S. Abbasbandy, R. Naz, T. Hayat, and A. Alsaedi, "Numerical and analytical solutions for Falkner–Skan flow of MHD Maxwell fluid," Appl. Math. Comput. 242, 569–575 (2014).
[7]. M. Mustafa, J. A. Khan, T. Hayat, and A. Alsaedi, "Simulations for Maxwell fluid flow past a convectively heated exponentially stretching sheet with nanoparticles," AIP Adv. 5(3), 037133 (2015).
[8]. M. Awais, T. Hayat, S. Irum, and A. Alsaedi, "Heat generation/absorption effects in a boundary layer stretched flow of Maxwell nanofluid: Analytic and numeric solutions," PLoS One 10(6), e0129814 (2015).
[9]. M. Ramzan, M. Bilal, J. D. Chung, and U. Farooq, "Mixed convective flow of Maxwell nanofluid past a porous vertical stretched surface—An optimal solution," Results Phys. 6, 1072–1079 (2016).
[10]. K.S. Adegbie , A.J. Omowaye, A.B. Disu, I.L. Animasaun, Heat and mass transfer of upper convected Maxwell fluid flow with variable thermo-physical properties over a horizontal melting surface. Appl Math (2015) 6(08):1362–79. doi:10.4236/am.2015. 68129
[11]. M. Mustafa, T. Hayat, A. Alsaedi, Rotating flow of Maxwell fluid with variable thermal conductivity: An application to non-fourier heat flux theory. Int J Heat Mass Transfer (2017) 106:142–8. doi:10.1016/j.ijheatmasstransfer. 2016.10.051
[12]. Z. Shafique, M. Mustafa, A. Mushtaq, Boundary layer flow of Maxwell fluid in rotating frame with binary chemical reaction and activation energy. Results Phys (2016) 6:627–33. doi:10.1016/j.rinp.2016.09.006
[13]. J.O. Olabode, A.S. Idowu, M.T. Akolade, E.O. Titiloye, Unsteady flow analysis of Maxwell fluid with temperature dependent variable properties and quadratic thermosolutal convection influence. Partial Differential Equations Appl Math (2021) 4:100078. doi:10.1016/j.padiff.2021.100078
[14]. M.M. Heyhat, N. Khabazi, Non-isothermal flow of Maxwell fluids above fixed flat plates under the influence of a transverse magnetic field. J Mech Eng Sci (2011) 225(4): 909–16. doi:10.1243/09544062JMES2245
[15]. A.C. Venkata Ramudu, K. Anantha Kumar, V. Sugunamma, N. Sandeep, Heat and mass transfer in MHD Casson nanofluid flow past a stretching sheet with thermophoresis and Brownian motion. Heat Transfer. 2020; 1–18. https://doi.org/10.1002/htj.21865

[16]. H. Sadia, N. Gul, A. Zeb, Z.A. Khan, Convection heat–mass transfer of generalized Maxwell fluid with radiation effect, exponential heating, and chemical reaction using fractional Caputo–Fabrizio derivatives. Open Phys (2022) 20(1):1250–66. doi:10.1155/ 2022/3629416

[17]. A.V. Shenoy, Non-Newtonian fluid heat transfer in porous media. In Adv Heat transfer (1994) 24. 101–90

[18]. Maatoug, K. Samah, K. Hari Babu, V. V. L. Deepthi, K. Ghachem, K. Raghunath, G. Charankumar, and Sami Ullah Khan. Variable chemical species and thermo-diffusion Darcy–Forchheimer squeezed flow of Jeffrey nanofluid in horizontal channel with viscous dissipation effects, Journal of the Indian Chemical Society 100, no. 1 (2023): 100831. https://doi.org/10.1016/j.jics.2022.100831

[19]. Bafakeeh, T. Omar, K. Raghunath, Farhan Ali, Muhammad Khalid, El Sayed Mohamed Tag-ElDin, Mowffaq Oreijah, Kamel Guedri, Nidhal Ben Khedher, and Muhammad Ijaz Khan. "Hall current and Soret effects on unsteady MHD rotating flow of second-grade fluid through porous media under the influences of thermal radiation and chemical reactions." Catalysts 12, no. 10 (2022): 1233. https://doi.org/10.3390/catal12101233

[20]. V.V.L. Deepthi, Maha MA Lashin, N. Ravi Kumar, K. Raghunath, Farhan Ali, Mowffaq Oreijah, Kamel Guedri, El Sayed Mohamed Tag-ElDin, M. Ijaz Khan, and Ahmed M. Galal. "Recent development of heat and mass transport in the presence of Hall, ion slip and thermo diffusion in radiative second grade material: application of micromachines." Micromachines 13, no. 10 (2022): 1566. https://doi.org/10.3390/mi13101566

[21]. G. Aruna, K. Hari Babu, B. Venkateswarlu, and K. Raghunath, An unsteady MHD flow of a second-grade fluid passing through a porous medium in the presence of radiation absorption exhibits Hall and ion slip effects, Heat Transfer (2023). https://doi.org/10.1002/htj.22716

[22]. K. Raghunath, R. Mohanaramana, G. Nagesh, G. Charankumar, Sami Ullah Khan, and M. Ijaz Khan. "Hall and ion slip radiative flow of chemically reactive second grade through porous saturated space via perturbation approach." Waves in Random and Complex Media (2022): 1-17. https://doi.org/10.1080/17455030.2022.2108555

[23]. K. Raghunath, G. Charankumar, and L. Giulio. "Effects of Soret, rotation, Hall, and ion slip on unsteady MHD flow of a Jeffrey fluid through a porous medium in the presence of heat absorption and chemical reaction." J. Mech. Eng. Res. Dev 45, no. 3 (2022): 80-97.

[24]. K. Raghunath, and R. Mohanaramana. "Hall, Soret, and rotational effects on unsteady MHD rotating flow of a second-grade fluid through a porous medium in the presence of chemical reaction and aligned magnetic field." International Communications in Heat and Mass Transfer 137 (2022): 106287. https://doi.org/10.1016/j.icheatmasstransfer.2022.10628